Round Turbulent Air Jet Submitted to a Pulsed Coflow

Marc Saudreau, Jacques Borée, Yannick Bury, Georges Charnay

Round Turbulent Air Jet Submitted to a Pulsed Coflow

M. Saudreau*
Centre National de la Recherche Scientifique, 31400 Toulouse, France
J. Borée†
Ecole Nationale Supérieure de Mécanique et d'Aérotechnique, 86 961 Futuroscope-Chasseneuil, France
and
Y. Bury‡ and G. Charnay§
Centre National de la Recherche Scientifique, 31400 Toulouse, France

Mean and turbulent properties of an unsteady round air jet submitted to a pulsed coflowing airstream were studied from laser Doppler Velocimetry measurements. The ejection velocity of the jet is kept at a constant value, whereas the coflowing stream is pulsed. These measurements revealed that the unsteadiness leads to a longitudinal partition of the jet. Near the jet exit, the flow is a quasi-steady jet flow. Farther downstream, the flow is unsteady with the creation of a large and propagative structure in the jet flow. The objective of the study is comprehensive understanding of the main physical mechanisms induced by the coflow unsteadiness. Consequences of the entrainment process are also discussed.

Nomenclature

C_{el}	=	entrainment coefficient
Ct	=	Craya–Curtet number (see Ref. 7)
D	=	jet exit diameter, 4 mm
D^*	=	equivalent source diameter
f	=	pulsation frequency, 75 Hz
g	=	acceleration of the gravity field
I_u	=	streamwise turbulent intensity
I_v	=	radial turbulent intensity
K	=	anisotropic parameter
k	=	turbulent kinetic energy
$l(z, t)$	=	jet half-width
$M_e(t)$	=	initial excess momentum flux
$\dot{m}_e(t)$	=	relative radial mass flux
P	=	pressure field
Sr	=	Strouhal number, $t_{\text{adv}}/t_{\text{puls}}$
T	=	pulsation period, $1/2\pi f$
t_{adv}	=	mean advection timescale
t_{diff}	=	turbulent diffusion timescale
t_k	=	unsteady variation of k timescale, $[1/k(\partial k/\partial t)]^{-1}$
t_{puls}	=	pulsation timescale, $1/2\pi f$
t_{sub}	=	timescale of the turbulent energy transfer
U	=	longitudinal velocity (z direction)
$\bar{U}$	=	mean part of U
u	=	fluctuation part of U
u'	=	$(\overline{uu})^{1/2}$
V	=	radial velocity (r direction)
V_0	=	front velocity
$\bar{V}$	=	mean part of V
v	=	fluctuation part of V
W	=	azimuthal velocity (θ direction)
$\bar{W}$	=	mean part of W
w	=	fluctuation part of W
(z, r, θ)	=	cylindrical coordinate system
ϵ	=	dissipation rate of k
θ	=	jet momentum radius
τ	=	turbulent timescale, k/ε
$\langle\cdot\rangle$	=	average value over one period:

$$\left(\frac{1}{T}\int_0^T \cdot \, \mathrm{d}t\right)$$

Subscripts

cl	=	centerline values
jet	=	jet exit conditions
∞	=	coflowing stream

Superscripts

jet	=	jet exit conditions
0	=	steady value
.	=	time derivative, $\partial./\partial t$
$-$	=	phase-averaged value

Introduction

THE understanding and modeling of unsteady flows submitted to external excitation are a challenges for the control and optimization of many industrial processes. Models that attempt to predict unknown complex turbulent flows need to be evaluated using measurements and physical analysis in basic flows before they can be applied in a general case. In this respect, the unsteady axisymmetric jet is a model nonhomogeneous turbulent flow that exhibits entrainment and mixing phenomena and has many practical applications. A large amount of research has been devoted to static or dynamic control of free or coflowing jets. (See the recent reviews by Johary and Paduano[1] and Fiedler.[2]) These studies are of high practical interest to control the level of external entrainment (large-scale effect), of mixing (small-scale effect), and of noise production (large-scale effect). However, these efforts have focused on jet exit conditions with various types of modulations: harmonic, nonharmonic, and low-amplitude and high-amplitude pulses.[1,3] To the authors' knowledge, less attention has been paid to the unsteadiness of the surrounding atmosphere of the jet. This is quite surprising

*Ph.D. Student, Institut de Mécanique des Fluides de Toulouse, UMR Institut National Polytechnique de Toulouse-UPS 5502; currently Postdoctoral Researcher, European Center for Research and Advanced Training in Scientific Computation, 42 Avenue Gaspard Coriolis, 31057 Toulouse Cedex, France; saudreau@cerfacs.fr.

†Professor, Laboratoire d'Etudes Aérodynamique, 1 Avenue Clement Ader.

‡Research Engineer, Institut de Mécanique des Fluides de Toulouse, UMR Institut National Polytechnique de Toulouse-UPS 5502, Avenue Camille Soula.

§Senior Researcher, Institut de Mécanique des Fluides de Toulouse, UMR Institut National Polytechnique de Toulouse-UPS 5502, Avenue Camille Soula.

because such unsteadiness is relevant in many industrial applications. One such application is, for example, in the intake port of spark ignition engines of natural gas vehicles. There, the injected gaseous fuel is submitted to a pulsed airflow, where acceleration can reach values of $\pm 3000\ g$. In this severe situation, taking into account the unsteadiness of the surrounding atmosphere and the flow nonhomogeneity is particularly important to describe the mixing.[4] Unsteady nonhomogeneous situations are particularly challenging because the phase-averaged baroclinic torque competes with the mean shear. To understand such complex flows, an unsteady homogeneous situation has to be considered first to evaluate unsteady effects.

The purpose of the present paper is to report on the dynamics induced by the unsteadiness of an airstream coflowing on an air jet. The case discussed here is believed to be a model configuration because both jet flow and external stream are aligned. Moreover, the ejection velocity of the jet is kept at a constant value. Phase-averaged mean and turbulent properties of the unsteady homogeneous flow are presented and compared to the steady jet in coflow. A physical analysis is proposed to provide a better understanding of the time and spatial development of the imposed perturbation along the jet flow. Finally, the modification of the entrainment process is discussed.

Experiment

Flow Bench

The experiments[5] were conducted in a square duct with a total length of 2.30 m and a cross section of $60 \times 60\ \text{mm}^2$ (Fig. 1). To perform optical measurements in the upstream part of the duct, the test section was equipped with transparent sides 128 mm long (Fig. 2). The upstream duct entrance opens out into ambient air, and the downstream duct end succeeds to a vacuum pump. Because of a motorized butterfly valve located upstream of the vacuum pump, the air channel flow is generated and pulsed at a frequency of $f = 75$ Hz. Pulsation is tuned with the channel acoustics and corresponds with a half-wave mode. Both duct extremities are pressure nodes so that for about 30 jet diameters downstream the duct inlet, including the test section, the coflow velocity U_∞ is quasi uniform and varies from 5 to 30 m/s with time (Fig. 3). Resulting values of acceleration/deceleration $\dot{U}_\infty$ rise from $+400$ to $-700\ g$. With a grid and a convergent-type collector placed upstream, the test section provides a flat velocity profile during the pulsation and a turbulent intensity of 1.5%.

A 4-mm-diam cylindrical tube placed in the center of the duct allows the generation of the air jet. A sonic nozzle is inserted in the tube. It is located 10 cm (25 diameters) upstream from the exit of the tube to obtain a developed pipe flow of axial velocity equal to $U_{\text{jet}} = 60\ \text{ms}^{-1}$. To fix the jet exit velocity in the time-varying pressure field, one has to keep the volume in the tube downstream the sonic nozzle at a minimum. In the present setup, the measured fluctuations of the jet exit velocity are lower than 3% (Ref. 5). The Reynolds number based on jet exit diameter and air viscosity is 1.7×10^4.

Measurement Techniques

Two-component laser Doppler velocimetry (LDV; Dantec BSA) is used and adapted to unsteady conditions. A description of the parameters of the system is given in the Appendix. Note that a Dantec

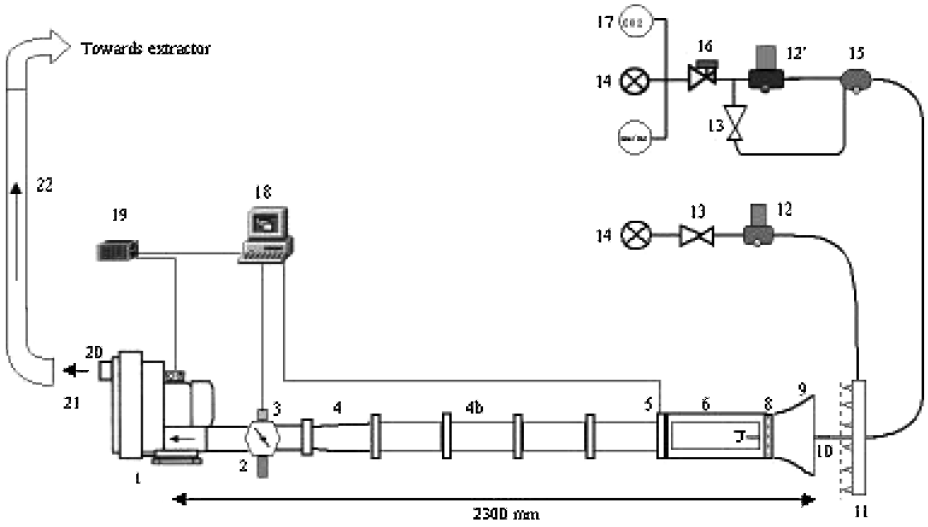

Fig. 1 Experimental setup: 1) vaccum pump, 2) motorized butterfly, 3) encoder, 4) diffuser, 4b) duct module, 5) pressure sensor, 6) test section, 7) coaxial jet, 8) turbulence generating grid, 9) convergent-type collector, 10) sonic nozzle, 11) "spider" seeding diffusor, 12) seeding system, 12') pressurised seeding system, 13) flow control valve, 14) compressed air, 15) pressure measurement chamber, 16) electropneumatic servocontrol valve, 17) CO_2 or He/N_2 mixing pressurized gas, 18) parameter control computer, 19) radio frequency interference (RFI) filter equipped rotation speed switch, 20) exhaust, 21) buffer zone, and 22) exhaust circuit.

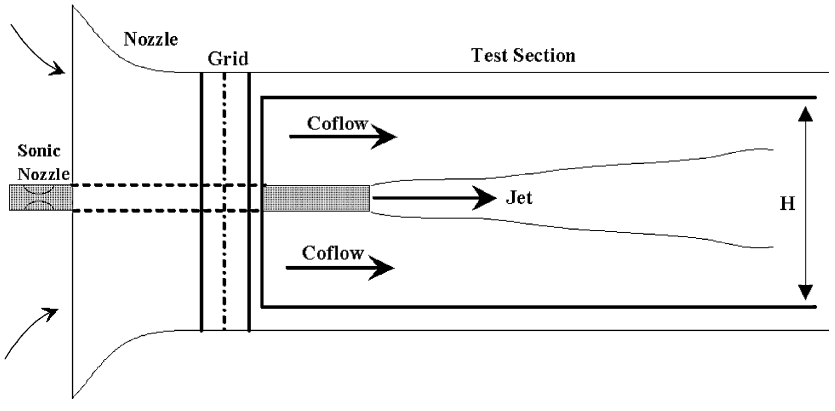

Fig. 2 Test section.

55X12 beam expander is used to reduce the size of the measurement volume. The receiving optics are settled at a 20-deg off-axis angle from the incident beam to minimize the contribution of optical noise. A systematic study of the sensitivity of statistical moments and data rate to the parameters of the system was performed in Bury.[5] Two original regulated oil seeding systems were specially designed for the experiment. To limit the measurement bias[6] associated with non-homogeneous seeding, we have achieved equal coflow and jet seeding rates. The diameter of the olive oil seeds is on the order of 1 μm. Their time constant is, thus, $\tau_p \approx 3.10^{-6}$ s. We have verified that they are able to track accurately the turbulent flow in the present experiment. For example, 10 jet diameters downstream, and even in the most severe situation corresponding to the highest shear in the coflowing jet, one can easily estimate the ratio between this time constant and the Kolmogorov timescale. This Stokes number is lower than 0.2. The droplets are, thus, able to track all of the scales of the turbulent motion relevant for the present study.

To perform ensemble averaging, an encoder is connected to the motorized butterfly valve. If we denote by an overbar $\bar{U}$ the phase average of instantaneous quantity U at a particular phase t in the period T of the pulsation, then

$$\bar{U}(\boldsymbol{x}, t) = \lim_{N \longrightarrow +\infty} \frac{1}{N} \sum_{i=1}^{N} U(\boldsymbol{x}, t + iT) \tag{1}$$

The turbulence field is then deduced from the deviation between instantaneous and previous phased-average fields: $u(\boldsymbol{x}, t) = U(\boldsymbol{x}, t) - \bar{U}(\boldsymbol{x}, t)$. In our case, more than $N = 500$ samples per encoder degree have been used to average the LDV data. Consequently, estimated statistical absolute errors for mean and u' values are $\Delta\bar{U} \approx 0.1 \cdot u'$ and $\Delta u' \approx 0.06 \cdot u'$, respectively, with a 95% confidence level. Therefore, even in the most severe situation, which corresponds to the highest turbulence intensity, maximum $(u/\bar{U}) \approx 30\%$, the relative errors for mean and standard deviation values are always lower than $E_{\bar{U}} \leq 3\%$ and $E_{u'} \leq 6\%$.

Longitudinal profiles from 0 to 25 jet diameters and radial profiles at 0, 5, 10, 15, and 20 diam downstream of the jet outlet were measured. Measurements were performed under the four following coflow conditions: unsteady coflow and steady coflow at, respectively, $\bar{U}_\infty = 5$, 17.5, and 30 m/s, which correspond to unsteady phases A (0 deg), B (40 deg), C (75 deg), and D (142 deg) in Fig. 3.

In regard to coflow velocities investigated, the duct radius has been calculated to avoid any recirculation due to confinement. Craya–Curtet number (see Ref. 7) Ct permits the evaluation of the influence of the confinement. If $Ct > 0.8$, the jet entrainment is not modified by the external wall and recirculation does not appear. In the worst situation, Craya–Curtet number Ct based on experimental initial condition is 1.5. Measurements have also confirmed that confinement can be neglected.[5]

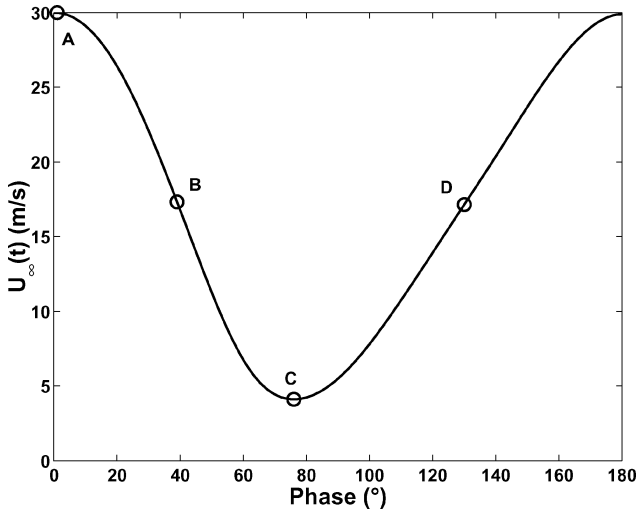

Fig. 3 Phase evolution of the coflow velocity U_∞: A, $U_\infty(t)$ = 30 m/s; B, $U_\infty(t)$ = 17.5-m/s deceleration; C, $U_\infty(t)$ = 5 m/s; and D, $U_\infty(t)$ = 17.5-m/s acceleration.

The flow will be described henceforth using a cylindrical coordinate system (z, r, θ) to indicate the axial, radial, and azimuthal directions. The origin is set at the tube exit and at the center of the inner jet. The components of the instantaneous velocity field are denoted by U, V, and W. No mean swirling motion was detected to within our measurement precision ($W \equiv 0$). The components of the instantaneous fluctuating velocity field are denoted by u, v, and w. As in Eq. (1), an overbar denotes Reynolds phase averaging.

Experimental Results

Steady Coflowing Jet

The flow bench was validated in a steady situation. To do so, three coflow velocities, $\bar{U}_\infty^0 = 5$, 17.5, and 30 m/s, have been investigated. It is well known that a jet surrounded by a moving stream develops in a different manner that a jet issuing in a quiet atmosphere.[8] An important parameter introduced by dimensional considerations is the momentum radius of the jet θ:

$$\rho_\infty \left(\bar{U}_\infty^0\right)^2 \theta^2 = \int\int \rho \bar{U}^0 \left(\bar{U}^0 - \bar{U}_\infty^0\right) 2\pi r \, \mathrm{d}r = M_e \tag{2}$$

where M_e is the integral excess momentum flux of the jet. When external volume forces are negligible, the integral excess momentum flux M_e is constant in the entire jet. Then θ is only determined by jet exit conditions. The similarity concept allows us to express the evolution of the excess velocity on jet axis $\bar{U}_{\mathrm{cl}}^0(z) - \bar{U}_\infty^0$, as follows[9]:

$$\lambda = F(z/\theta)$$

where

$$\lambda = \left(\bar{U}_{\mathrm{cl}}^0(z) - \bar{U}_\infty^0\right) \Big/ \bar{U}_\infty^0 \tag{3}$$

For fixed initial conditions, that is, $\theta = C^{te}$, the flow evolves from a jet, $\lambda \sim (z/\theta)^{-1}$, near the jet exit ($z/\theta \to 0$) to a jet wake, $\lambda \sim (z/\theta)^{-2/3}$, farther downstream ($z/\theta \to \infty$). Recent experimental results of Nickels and Perry[10] have shown that the distance where the transition from the jet to jet wake occurs is about $z/\theta \sim 10$. These authors have proposed the following law to describe the longitudinal evolution of λ:

$$\lambda = \frac{C\left(A_1 + (z/\theta)^2\right)^{\frac{1}{6}}}{z/\theta} \tag{4}$$

where $C = 2.67$ and $A_1 = 299$.

Figure 4 shows that our measurements are in good agreement with the results of Nickels and Perry.[10] As the coflow velocity increases, the decaying law of the excess velocity on the flow axis goes from $(z/\theta)^{-1}$ for $z/\theta < 10$ to $(z/\theta)^{-2/3}$ for $z/\theta > 10$. To our knowledge, the small difference with the Nickels and Perry law is due to exit conditions because at $25D$ we expect an influence on the flow development. Nickels and Perry used a quasi-top-hat profile for excess velocity at the jet exit, but our profiles are close to a fully turbulent pipe flow. In Fig. 5, the evolution of normal Reynolds stresses ($\overline{uu}^0$, $\overline{vv}^0$) on the jet axis is shown. Consider the longitudinal fluctuation intensity $I_u = (\overline{uu}^0)^{1/2}/[\bar{U}_{\mathrm{cl}}^0(z) - \bar{U}_\infty^0]$ on the jet axis. Near the jet exit, the flow changes from tube flow to jet flow and the turbulence is maximum at the end of the potential core. Farther downstream, the mean velocity gradient decreases and the production of longitudinal turbulence diminishes and is balanced by losses due to viscous dissipation and redistribution to the radial fluctuation. At this stage, if equilibrium exists, then $I_u = (\overline{uu}^0)^{1/2}/[\bar{U}_{\mathrm{cl}}^0(z) - \bar{U}_\infty^0]$ and $I_v = (\overline{vv}^0)^{1/2}/[\bar{U}_{\mathrm{cl}}^0(z) - \bar{U}_\infty^0]$ might reach asymptotic values. This state does not appear in Fig. 5 because our maximal downstream distance $z/D = 25$ is not sufficient to reach such a self-preserving state. Nevertheless, for cases $\bar{U}_\infty^0 = 5$ and 17.5 m/s, I_u (respectively I_v) tends to approach experimental values of 0.27 (respectively 0.24) obtained by Wygnansky and Fiedler[11] and Hussein et al.[12] It appears also that the $\bar{U}_\infty^0 = 30$ m/s case is clearly different from the others because $I_u \approx 0.37$ and $I_v \approx 0.32$. Turbulent intensities are nearly

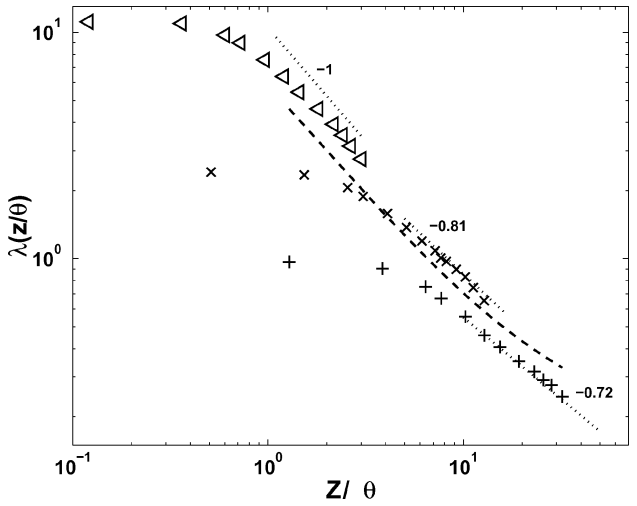

Fig. 4 Decay of the axial excess velocity, $\lambda = F(z/\theta)$, for ◁, U_∞ = 5 m · s^{-1} ×, U_∞ = 17.5 m · s^{-1}; +, U_∞ = 30 m · s^{-1}; and - - - -, Nickels and Perry results.[10]

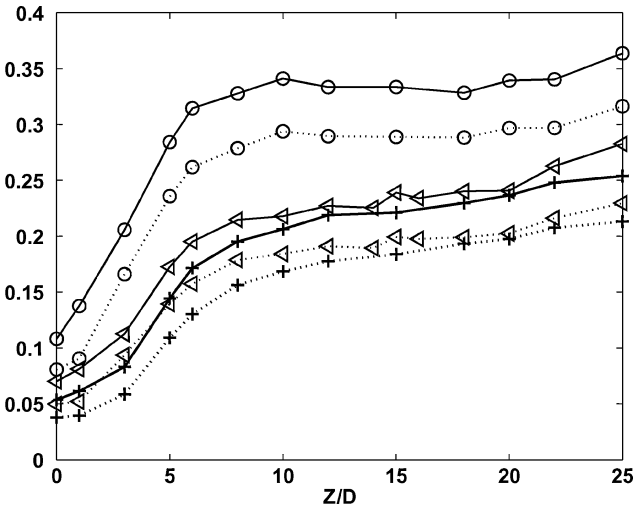

Fig. 5 Axial evolution of ——, $(\overline{uu})^{1/2}/[\bar{U}_{cl}(z) - \bar{U}_\infty]$; . . . , $(\overline{vv})^{1/2}/[\bar{U}_{cl}(z) - \bar{U}_\infty]$; at +, U_∞ = 5 m · s^{-1}; ◁, U_∞ = 17.5 m · s^{-1}; and ○, U_∞ = 30 m · s^{-1}.

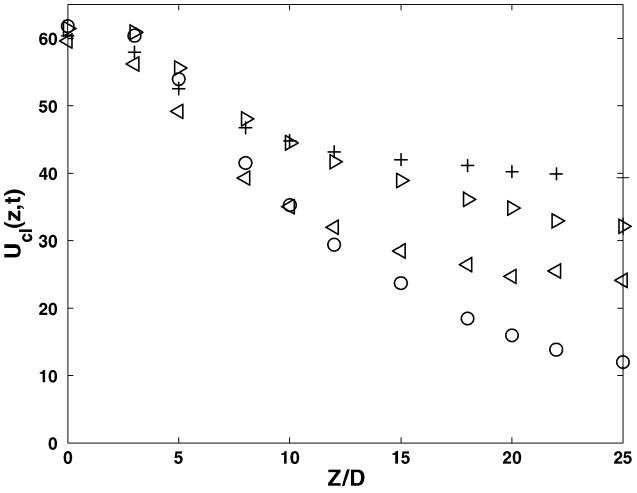

Fig. 6 Axial velocity decay $U_{cl}(z,t) = f(z/D)$; experimental unsteady results: +, phase A; ◁, phase B; ○, phase C; and ▷, phase D.

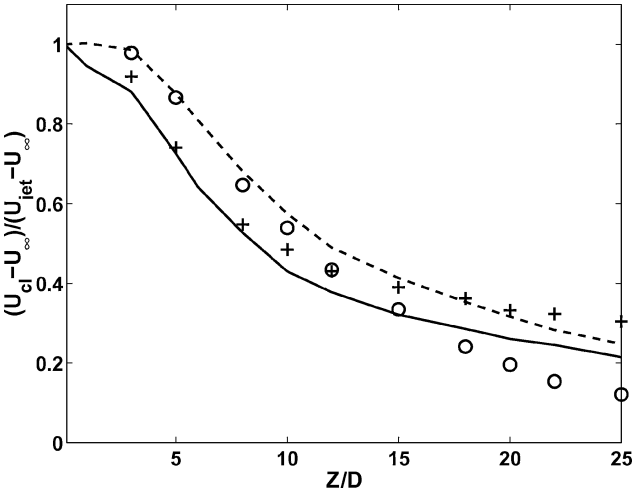

Fig. 7 Comparison of the axial velocity decay $U_{cl}(z, t)$ between steady and unsteady coflow at phases A and C; experimental unsteady cases +, phase A; ○, phase C; experimental steady cases ——, U_∞ = 30 m/s and - - -, U_∞ = 5 m/s.

two times larger than for the $\bar{U}^0_\infty = 5$ m/s case. Contrary to jet flow, there are no standard experimental values for jet-wake flow. Because of the advective process, the jet-wake flow, like wake flow, is very sensitive to initial conditions and may exhibit very different turbulent properties.[13] Nevertheless, these values agree very well with experimental results from studies of a jet with a coflowing stream because, from the review by Nickels and Perry,[10] I_u and I_v can vary from 0.27 to 0.48.

Unsteady Coflowing Jet

The phase-averaged mean axial velocity exhibits a very large-amplitude variation during the pulse (Fig. 6). At $z/D = 25$, the velocity goes from 40 m · s^{-1} at phase A to 12 m · s^{-1} at phase C. To bring to the fore the unsteady effects on the flow development, we have compared unsteady cases to steady ones for the same coflow velocity $\bar{U}_\infty(t)$. We focus first on the maximum (phase A) and the minimum (phase C) external velocities (Fig. 7). At the end of the deceleration phase (phase C), the mean velocity on the jet axis is much lower than even the associated steady situation. However, at the end of the acceleration phase (phase A), the mean velocity is a maximum on the axis and nearly corresponds to the steady evolution. The external velocity associated with phase B (maximum deceleration phase) and D (maximum acceleration phase) is $\bar{U}_\infty(t) = 17.5$ m · s^{-1} (Fig. 8). A remarkable feature is that the axial velocity decay law is more important during deceleration phase B than during acceleration phase D. Moreover, the axial evolutions at phases B and D clearly lie on both sides of the steady mean velocity decay.

The same trends are observed with the behaviors of normal stresses $\overline{uu}$ and $\overline{vv}$. We have noticed that $\overline{uu}$ and $\overline{vv}$ evolve in the same way except that, as in steady coflowing jets, the radial component has a lower intensity than the streamwise component.[10] Thus, only $\overline{uu}$ has been used to compare unsteady reasults with steady results (Fig. 9). At phase A, $\overline{uu}$ has values close to the steady case, $\bar{U}_\infty(t) = 30$ m/s. However, when the external velocity is a minimum (phase C), $\overline{uu}$ is the same as the steady case 5 m/s up to $z/D = 15$, but is clearly smaller farther downstream. Phase B and D correspond to the same external velocity, but not to the same acceleration. We again notice that $\overline{uu}$ differs significantly. The Reynolds stresses are much larger during the acceleration phase. At phase D and for $z/D > 20$, they are even larger than the largest values in the steady situation.

The response of the jet to the large-scale external perturbation is expected to be quite complex because its behavior is space and time dependent. Figures 6–9 only provide a view of the flow at a given phase. The phase evolution of the rescaled mean excess velocity

$$\frac{\bar{U}_{cl}(z,t) - \bar{U}_\infty(t)}{\max\left[\bar{U}_{cl}(z,t) - \bar{U}_\infty(t)\right]}$$

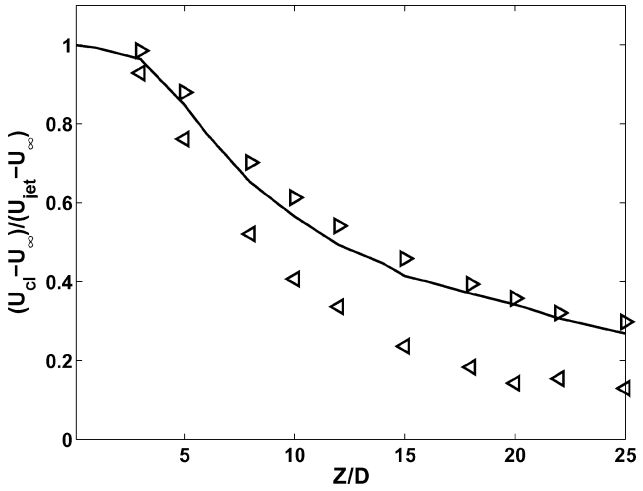

Fig. 8 Comparison of the axial velocity decay U_{cl} evolution between steady and unsteady coflow at phases B and D: experimental unsteady cases ◁, phase B; ▷, phase D; and experimental steady case ——, U_∞ = 17.5 m/s.

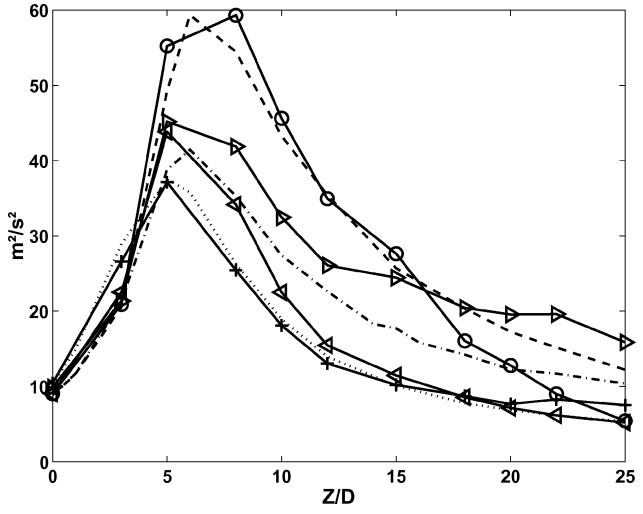

Fig. 9 Comparison of the axial evolution of $\overline{uu}$ between steady and unsteady coflow cases: experimental unsteady cases +, phase A; ◁, phase B; ○, phase C; and ▷, phase D; experimental steady cases - - -, U_∞ = 30 m/s; –·–, U_∞ = 17.5 m/s; and . . . , U_∞ = 5 m/s.

at $z/D = 0$, 5, 10, 15, and 20 clearly show the propagation of a perturbation (Fig. 10). Phase C is associated with a minimum external velocity and, thus, with a maximum mean excess velocity at the jet exit. No phase lag is observed up to $z/D = 10$, but farther downstream, a phase lag appears and increases with the downstream distance. Finally, the time derivative of the local mean velocity (Fig. 11) proves that the perturbation carried by the jet flow is evolving markedly as it propagates downstream. In particular, $\partial\bar{U}_{cl}/\partial t$ has a positive peak for $z/D > 15$ at the beginning of the acceleration phase. The phase of this peak shifts and its level increases as we move downstream.

Time evolution of the Reynolds stresses at $z/D = 25$ is shown in Fig. 12. During the deceleration phase, $\overline{uu}$ and $\overline{vv}$ are slowly decreasing. However, a very sharp increase is measured at the beginning of the acceleration phase. The phases corresponding to the maximum of $\partial\bar{U}_{cl}/\partial t$ and $\partial\overline{uu}_{cl}/\partial t$ are shown in Fig. 13. Figure 13 shows that this phenomenon propagates at a constant velocity of $V_0 \simeq 28$ m/s. Note in Fig. 12 that increases of $\overline{uu}$ and $\overline{vv}$ do not occur at the same phase and with the same intensity. Figure 14, which shows the anisotropic parameter $[K = (\overline{uu} - \overline{vv})/(\overline{uu} + \overline{vv})]$, confirms this observation. K is clearly a maximum when the rate of increase $\partial\overline{uu}/\partial t(z,t)$ is maximum and not when $\overline{uu}$ is a maximum. In such quasi-parallel turbulent flow, there is a direct link between

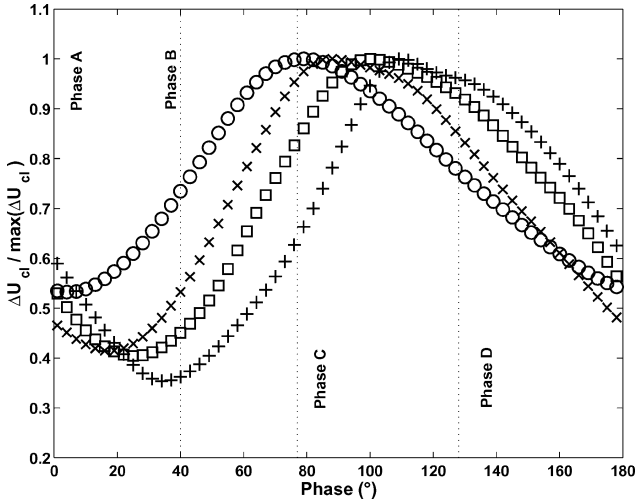

Fig. 10 Phase evolution of the mean excess axial velocity: ○, z/D = 10; ×, z/D = 15; □, z/D = 20; and +, z/D =22.

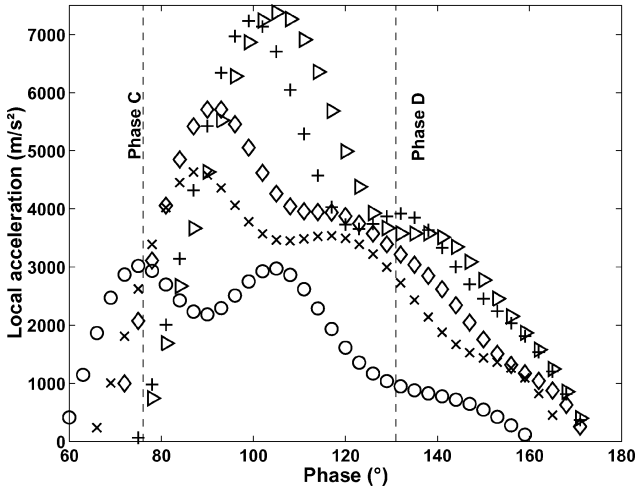

Fig. 11 Phase evolution of the axial acceleration $\partial\bar{U}_{cl}/\partial t$: ○, z/D = 10; ×, z/D = 15; ◇, z/D = 18; +, z/D = 22; and ◁, z/D = 25.

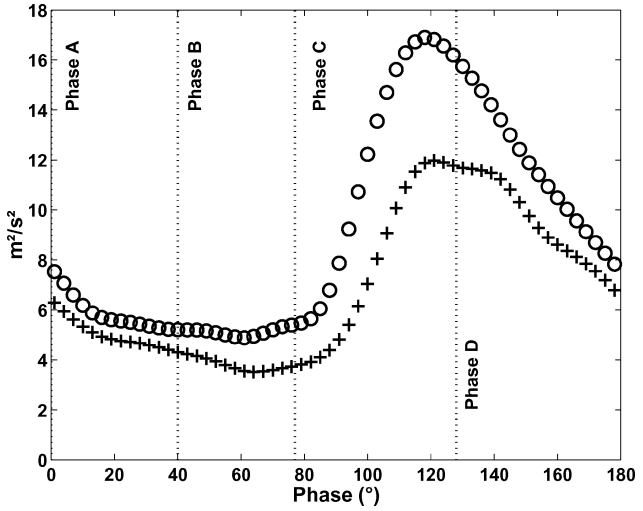

Fig. 12 Phase evolution of Reynolds stresses at z/D = 25 on jet axis: ○, $\overline{uu}$ and +, $\overline{vv}$.

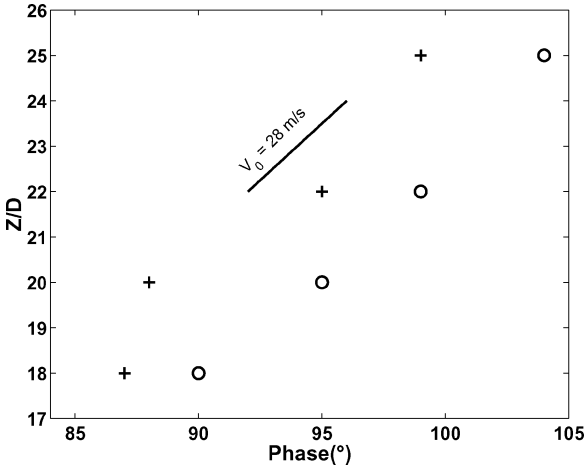

Fig. 13 Front velocity deduced from measurements: ○, $\partial \bar{U}_{cl}/\partial t$ and +, $\partial \overline{uu}_{cl}/\partial t$.

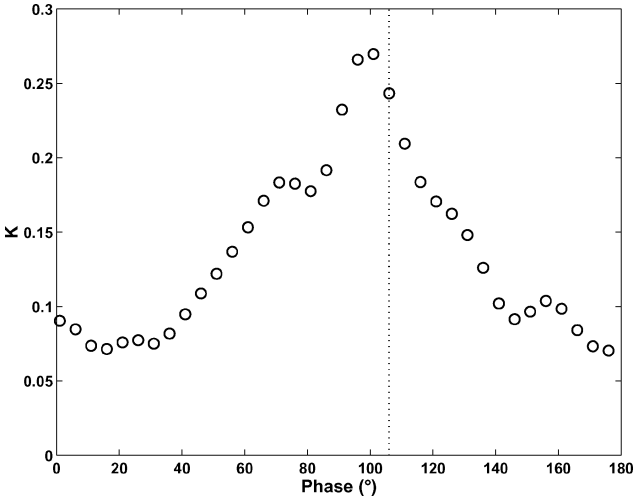

Fig. 14 Phase evolution of $K = (\overline{uu} - \overline{vv})/(\overline{uu} + \overline{vv})$ on jet axis at z/D = 25; . . . , front location.

the longitudinal Reynolds stress and the mean velocity field. Indeed, the entire production of kinetic energy occurs in the equation for $\overline{uu}$, whereas the transverse Reynolds stress $\overline{vv}$ receives its energy from the pressure interaction terms.[14] Saudreau[15] has shown that the evolution of the anisotropy (Fig. 14) is explained by a time delay between the production and the redistribution mechanisms. Therefore, this experiment can be useful to test the pressure rate of strain models in second-order modeling.[16]

The temporal evolution of the jet half-width $l(z,t)$ is presented in Fig. 15. Here, $l(z,t)$ is defined by

$$\frac{\bar{U}[l(z,t),t] - \bar{U}_\infty(t)}{\bar{U}_{cl}(t) - \bar{U}_\infty(t)} = 0.5$$

The relative variation of $l(z,t)$ is very large because $(l_{max} - l_{min})/\langle l \rangle \approx 70\%$ at $z/D = 20$. The jet half-width $l(z,t)$ is a minimum at the beginning of the deceleration phase and reaches a maximum at the beginning of the acceleration phase. The mean values $\langle l \rangle$ have been computed by averaging $l(z,t)$ over the whole cycle. We obtain $\langle l \rangle = 0.66D$ at $z/D = 10$ and $\langle l \rangle = 1.13D$ at $z/D = 20$. It is lower than the steady value measured for an external velocity of 17.5 m/s, which is $0.75D$ at $z/D = 10$ and $1.25D$ at $z/D = 20$. Thus, the mean evolution of the unsteady jet has nothing to do with the steady jet at the mean external velocity $\bar{U}_\infty(t) = 17.5$ m/s. The more important feature is that maximum values of $l(z,t)$ and $\partial \bar{U}_{cl}/\partial t$ occur at nearly the same time. A particular structure, corresponding to a large lateral coherence and a

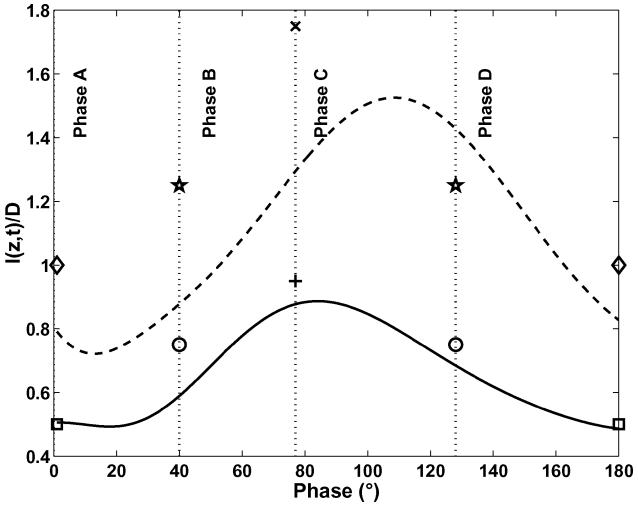

Fig. 15 Phase evolution of the jet half-width $l(z \cdot t)$: symbols are steady jets; ——, z/D = 10; and - - -, z/D = 20.

high temporal acceleration, therefore, propagates downstream at the beginning of the acceleration phase.

Physical Analysis

Timescale Analysis: Evaluation of Unsteady Effects

The behavior described seems to have some similarities with pulsed,[17,18] accelerated,[19] or starting freejets.[20] In these cases, the increase of the jet exit velocity, that is, the increase of the jet exit excess momentum flux $Me(t)$, leads to the formation of a large-scale structure that propagates and interacts with the downstream initial jet. This structure is strong enough to modify the entrainment process and the turbulent field. However, in our case the large coherent structure appears during the acceleration phase of the jet when the jet exit excess momentum flux $Me(t)$ decreases.

The variation of the coflowing stream has two main effects on the jet. First, it induces a time variation of the integral excess momentum flux at the jet exit $M_e(t)$ [Eq. (2)]. $M_e(t)$ decreases during the acceleration phase and increases during the deceleration phase. Second, the time variation of the coflow is driven by an alternative longitudinal pressure gradient that influences the entire flow. To deal with the jet response under these two effects, we have to refer to governing equations.

When classical hypotheses for quasi-parallel flows[14] are used, it is possible to show that the longitudinal mean momentum equation is

$$\underbrace{\frac{\partial}{\partial t}\bar{U}(z,t)}_{\text{unsteady}} + \underbrace{\bar{U}(z,t)\frac{\partial}{\partial z}\bar{U}(z,t) + \bar{V}(z,t)\frac{\partial}{\partial r}\bar{U}(z,t)}_{\text{advection}}$$

$$= \underbrace{-\frac{1}{\rho}\frac{\mathrm{d}\bar{P}_\infty}{\mathrm{d}z}(z,t)}_{\text{pressure}} + \underbrace{\frac{1}{\rho}\Sigma_T}_{\text{turbulence}} \qquad (5)$$

In the external region of the uniform coflow, because confinement effects can be neglected,[5] the momentum balance is simply

$$\rho_\infty \frac{\partial}{\partial t}\bar{U}_\infty(t) = -\frac{\mathrm{d}\bar{P}_\infty}{\mathrm{d}z}(z,t) \qquad (6)$$

In a constant density flow, that is, $\rho = \rho_\infty$, Eq. (5) finally becomes

$$\underbrace{\frac{\partial}{\partial t}\bar{U}(z,t)}_{t1} + \underbrace{\bar{U}(z,t)\frac{\partial}{\partial z}\bar{U}(z,t) + \bar{V}(z,t)\frac{\partial}{\partial r}\bar{U}(z,t)}_{t2}$$

$$= \underbrace{\frac{\partial}{\partial t}\bar{U}_\infty(t)}_{t3} + \underbrace{\frac{1}{\rho}\Sigma_T}_{t4} \qquad (7)$$

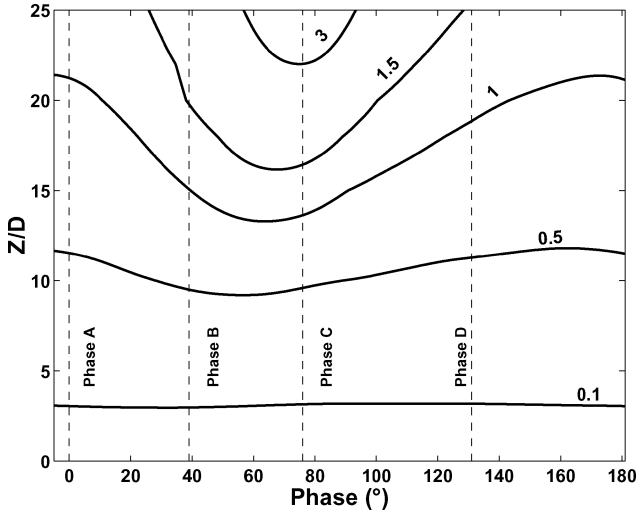

Fig. 16 Spatial and phase evolutions of t_{jet}/t_{puls} during one pulsation.

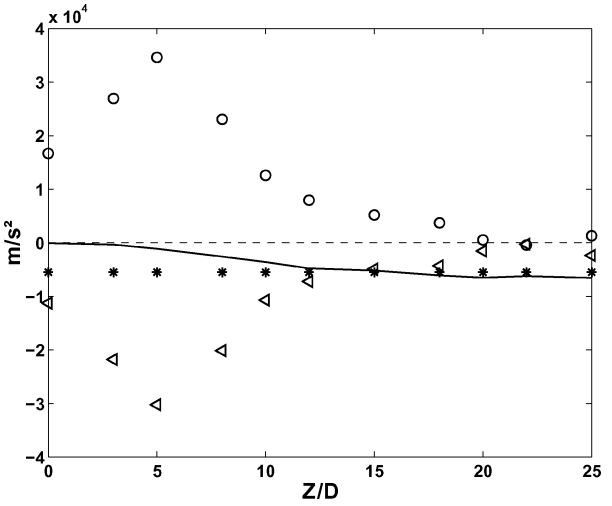

Fig. 17 Balance of momentum equation on jet axis at phase 45 deg; experimental unsteady results: ——, $t1$; ○, $t2$; ∗, $t3$; and ◁, $t4$.

If we consider the jet axis ($r = 0$), Eq. (7) is

$$\underbrace{\frac{\partial}{\partial t}\bar{U}_{\mathrm{cl}}(z,t)}_{t1} = -\underbrace{\bar{U}_{\mathrm{cl}}(z,t)\frac{\partial}{\partial z}\bar{U}_{\mathrm{cl}}(z,t)}_{t2} + \underbrace{\frac{\partial}{\partial t}\bar{U}_{\infty}(t)}_{t3} + \underbrace{\left[\frac{1}{\rho}\Sigma_T\right]_{r=0}}_{t4} \tag{8}$$

Equation (8) states that the time variation of mean momentum ($t1$) is due to the mean advection ($t2$), to the external imposed pressure gradient ($t3$), and to the turbulent diffusion ($t4$). Thus, the timescale variation of mean momentum in the flow is controlled by the advection timescale t_{adv}, by the pressure gradient timescale $t_{\mathrm{puls}} \simeq 1/2\pi f$, and by the turbulent diffusion timescale t_{diff}. In steady coflowing jets, mean advection and turbulent diffusion are in equilibrium and, therefore, have timescales of the same order of magnitude: $t_{\mathrm{adv}} \sim t_{\mathrm{diff}}$ (Ref. 16). Note that t_{adv} increases strongly vs axial distance [$t_{\mathrm{adv}} \approx z/U_{\mathrm{cl}} \approx (z/D)^2$ in a free steady jet]. In an unsteady situation, the pulsation timescale t_{puls} has to be taken into account, and the jet response then clearly results from a competition between the coflow variations imposed at the timescale t_{puls} and the mean advection timescale t_{adv}. The ratio $t_{\mathrm{adv}}/t_{\mathrm{puls}}$ is the local Strouhal number $Sr = z \cdot 2\pi f / U_{\mathrm{cl}}$:

1) If $t_{\mathrm{adv}} \ll t_{\mathrm{puls}}$, then the jet is quasisteady. The jet has enough time compared to the pulsation timescale to adapt to new exit conditions.

2) On the other hand, if $t_{\mathrm{adv}} \approx t_{\mathrm{puls}}$, the jet and the pulsation can interact strongly.

In the present situation, t_{adv} has been evaluated using $z/\overline{U_{\mathrm{cl}}}(t)$ and compared to t_{puls} during one pulsation (Fig. 16). The early development of the jet, $z/D \leq 10$, is quasisteady ($t_{\mathrm{adv}} \ll t_{\mathrm{puls}}$) whatever the phase. However, farther downstream, $z/D > 10$, an interaction of the pulsation with the jet is expected, particularly from phase B to phase D.

Phase-Averaged Balance of Mean Longitudinal Momentum on the Axis

Previous dimensional analysis has shown that the flow behavior depends on the axial distance from jet exit z/D and the pulsation phase. To deal more precisely with these spatiotemporal changes, evolutions of each term of Eq. (8) are presented in Figs.17–19. The first three terms have been deduced from measurements, and the turbulent term has been calculated from Eq. (8). When the axial evolution is considered, that is, the jet evolution at a fixed pulsation phase, the flow can be effectively separated in two parts (Fig. 17).

From $z/D = 0$ to $z/D \leq 15$, the advective term is mainly balanced by the turbulent diffusion term. This balance does not evolve significantly with time (Fig. 18); thus, in this region, the mean axial velocity budget corresponds to a quasi-steady jet[14] whatever the phase. In this region, the physical characteristics of the unsteady

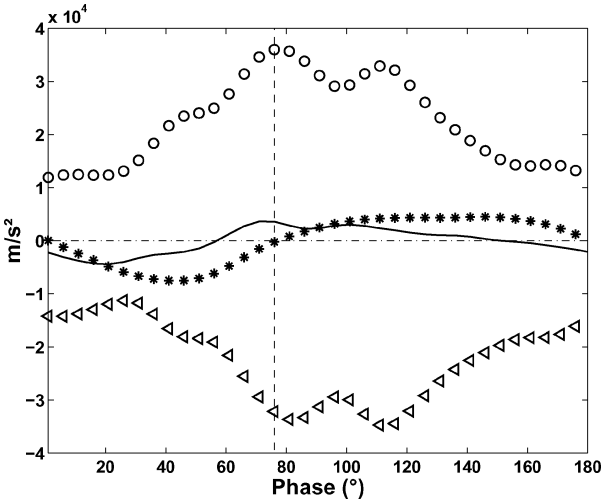

Fig. 18 Phase evolution of the mean momentum balance on the jet axis at z/D = 10; experimental unsteady results: ——, $t1$; ○, $t2$; ∗, $t3$; and ◁, $t4$.

flow do not differ from the corresponding steady jets. For example, decay laws of the axial velocity are identical (Figs. 7 and 8).

However, the balance of the downstream region, $z/D > 15$, differs strongly from that of a steady jet (Fig. 17). Time evolution of each term at a fixed downstream distance (Fig. 19) shows that the mean balance is more complex because it changes at any phase:

1) During the deceleration phase, the mean advection and turbulent transport terms are very weak. The unsteady term is only balanced by the acceleration term: $(\partial/\partial t)\bar{U}(z,t) \sim (\partial/\partial t)\bar{U}_{\infty}(z,t)$. At a fixed downstream distance and during these phases, the jet flow and the coflowing stream, thus, evolve in the same way and the mean excess velocity $\bar{U}(z,r,t) - \bar{U}_{\infty}(z,t)$ is constant in time.[15] Note that the turbulent diffusion and the longitudinal advection are negligible during this process with $t_{\mathrm{puls}} \ll t_{\mathrm{diff}}$ and $t_{\mathrm{puls}} \ll t_{\mathrm{adv}}$.

2) The beginning of acceleration phase is characterized by a strong increase of the advection term with a maximum at the phase 105 deg. At this phase, the evolution of the local acceleration $(\partial/\partial t)\bar{U}_{\mathrm{cl}}(z,t)$ is associated with the mean advective process. The mean advection is then responsible for the peak value of $(\partial/\partial t)\bar{U}(z,t)$ observed in Fig. 11. We, therefore, understand that the large-scale structure is created by the increase of the upstream fluid velocity and that this particular event is propagative.

At the end of the acceleration phase the three right-hand-side terms of the momentum balance equation have the same order of magnitude.

Entrainment of External Fluid in the Unsteady Jet

In most industrial configurations, jets are used to provide efficient mixing between the jet flow and the ambiant air. The mechanism of mixing can be divided in three steps.[21] First, the rollup of the large eddies of the jet flow leads to an engulfment of irrotational ambiant fluid into the inner turbulent jet flow. This is the entrainment process. Second, the vortex stretching reduces the scale of the entrained fluid to the viscous scale. Third, the mixing between the outer fluid and the jet fluid occurs at the molecular level. In our case, we are interested in large-scale effects, as in the entrainment process. Previous studies of pulsed or accelerated jets have already pointed out that the entraiment can be modified with high-amplitude velocity fluctuations.[3,17] In the case of accelerated jets,[19] experimental visualizations have shown that the creation of a large structure is associated with a strong reduction of the entrainment. From dimensional considerations,[22] it can be shown that the vortex has a finite volume entrainment appetite that results from engulfment of ambient fluid (process B; Fig. 20) and incorporation of overtaking fluid from the rear (process A; Fig. 20). During the acceleration, the vortex propagates and increases solely by incorporation of nozzle fluid from behind (process A). With less ambient fluid entering it, little entrainment could occur within the vortex. In our case, the large-scale structure is created by the increase of the upstream fluid velocity. The upstream fluid parcels catch up with the slower downstream fluid particles, and a large eddy is created as in starting jets.[20] No measurements of a passive scalar were made during the experiment. Unsteady Reynolds averaged Navier–Stokes (URANS) computations using second-order modeling have been performed by one of the authors.[15] Details of the computations are not described here for the sake of brevity. A passive scalar field resulting from the computation is shown in Fig. 21. The large-scale structure generated by the advective process appears very clearly in Fig. 21. URANS computations have clear limitations in the present context, and large eddy simulation should be a more appropriate way to capture the dynamics of the large-scale structures. However, the URANS approach provides good results if care is taken to satisfy the timescale separation between the mean flow and the residual turbulence.[23] Moreover URANS remains very helpful in the industry to keep computational cost reasonable. In the present situation, we were able to simulate the unsteady evolution of the mean velocity within 2% accuracy. From the numerical results, it is easy to compute the total amount of mass entrained in the jet structure during one period of the pulsation. At a given location z/D, the phase-averaged entrainment per unit lengh of external fluid in the jet structure, $\dot{m}_e$, is the relative radial mass flux at the moving location of the phase-averaged jet border:

$$\dot{m}_e(z,t) = -\int_{\partial l} \rho(V - V_j)\,\mathrm{d}l = \dot{m}(z,t) + \rho \dot{S}_j \qquad (9)$$

with

$$\dot{m} = -\int_{\partial l} \rho V\,\mathrm{d}l$$

where S_j is the time-dependent surface of the phase-averaged section of the jet at the given location and V_j is the radial

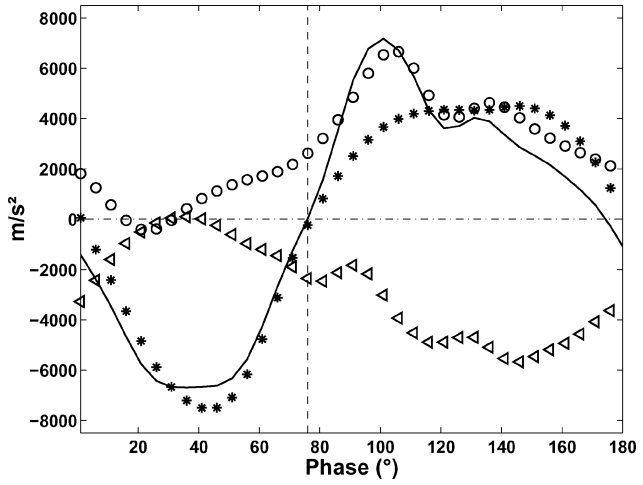

Fig. 19 Phase evolution of the mean momentum balance on the jet axis at $z/D = 22$; experimental unsteady results: ——, $t1$; ○, $t2$; ∗, $t3$; and ◁, $t4$.

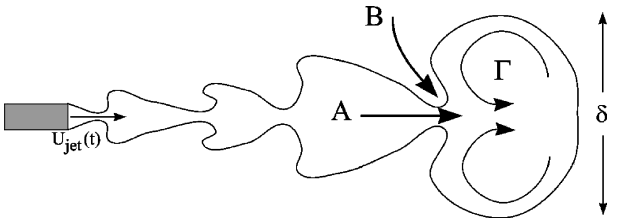

Fig. 20 Schematic of unsteady entrainment process during the acceleration phase.[22]

Table 1 Effect of coflow unsteadiness on jet entrainment

Z/D	$\dfrac{\langle \dot{m}_e(z)\rangle - \langle \dot{m}_e^{qs}(z)\rangle}{\langle \dot{m}_e^{qs}(z)\rangle}$
15	−0.0059
20	−0.051
25	−0.117

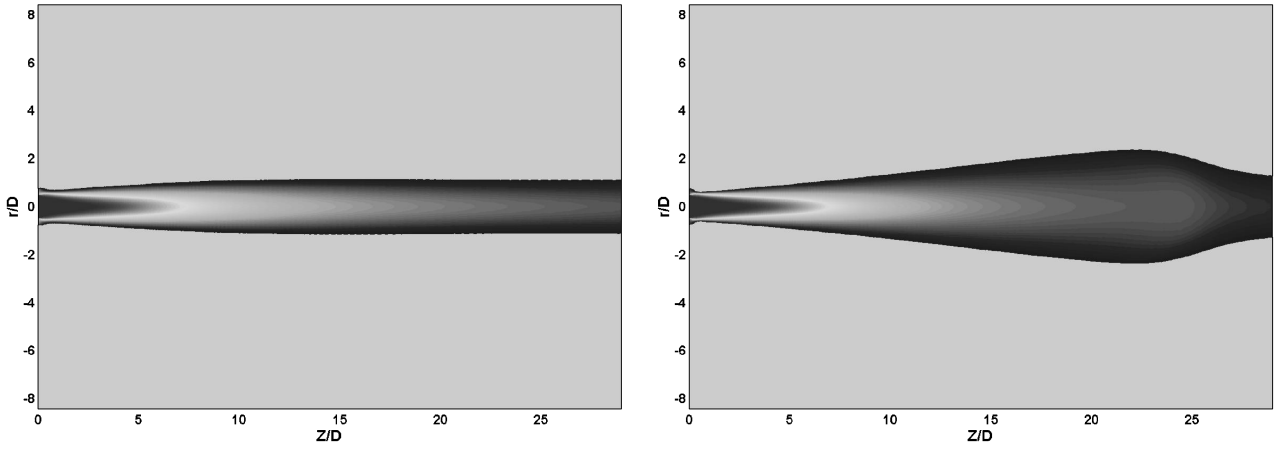

Fig. 21 Comparison of scalar field between a) deceleration phase phase B (45 deg) and b) acceleration phase when structure passes (117 deg).

displacement velocity of the jet contour. $\dot{S}_j$ is the time variation of S_j. For a periodic response of the excited jet,

$$\int_0^T \dot{S}_j \, \mathrm{d}t = [S_j(T) - S_j(0)] = 0$$

Thus, at the axial position z/D, the relative radial mass flux during one period is

$$\langle \dot{m}_e(z) \rangle = \frac{1}{T} \int_0^T \dot{m}_e(z,t) \, \mathrm{d}t = \frac{1}{T} \int_0^T \dot{m}(z,t) \, \mathrm{d}t \qquad (10)$$

To quantify the effect of the unsteadiness on the entrainment process, $\langle \dot{m}_e(z) \rangle$ is compared to the relative radial mass flux over one period obtained for a quasi-steady coflowing jet $\langle \dot{m}_e^{\mathrm{qs}}(z) \rangle$ in Table 1. The value of $\langle \dot{m}_e^{\mathrm{qs}}(z) \rangle$ has been computed from recent results of Donghee and Mungal[24] of the coflow effect on entrainment rate. At $Z/D = 15$, both flows are similar, but farther downstream, the mass of external fluid incorporated in the unsteady coflowing jet is lower (11% at $Z/D = 25$) than the amount that would be for a quasi-steady coflowing jet. Therefore, this work shows that the entrainment of external fluid in the jet is strongly reduced by the pulsed coflow.

Conclusions

An experimental investigation based on two-component LDV has been performed to study the dynamic behavior of a turbulent homogeneous jet submitted to a strongly pulsed coflow. A large part of this work was devoted to isolation and analysis of the influence of the unsteadiness on the development of the mean and turbulent fields. The unsteadiness leads to a longitudinal partition of the jet. Near the jet exit, the flow is a quasi-steady jet flow. Jet spreading rate, axial decaying laws, and turbulent intensities are similar to the corresponding steady coflowing jet. Farther downstream the flow is unsteady. Two remarkable features can be seen in this region. During the deceleration phase, the flow is driven by the pressure gradient in the duct. Velocity profiles, turbulent intensities, and the turbulent production rate process are constant in time. The flow seems to be frozen at the pulsation timescale. During the acceleration phase, a structure, similar to the structure observed in accelerated jets, develops at the end of the quasi-steady region. This structure propagates downstream and modifies considerably the turbulent fluctuations, as well as the spreading rate of the jet. We have also shown that the entrainment process is reduced.

In many industrial injection devices, the jet flow encounters an unsteady surrounding atmosphere. However, the influence of a surrounding fluid unsteadiness on the flow development has not received as much attention as variations of the jet ejection velocity. This study has shown that effects of the surrounding fluid unsteadiness are strong, as in the pulsed jet situation.

Appendix: Parameters of the LDV System

Table A1 Transmitting optics[a]

Parameter	Value
Gaussian beam diameter	1.4 mm
Focal length of the front lens	310 mm
Beam separation	73.7 mm
Diameter of the measurement volume	Green: 78 μm/blue: 74 μm
Length of the measurement volume	Green: 660 μm/blue: 620 μm
Fringe number	36
Fringe spacing	Green: 2.2 μm/blue: 2.1 μm
Shift frequency	40 MHz

[a]Colors of the beams, green for U velocity/blue for V velocity.

Table A2 Receiving optics

Parameter	Value
Off-axis angle	20 deg
Focal length of the front lens	300 mm
Diameter of the pinhole	100 μm
Magnification of the receiving optics	3
Effective length of the measurement volume	300 μm

Acknowledgments

The authors thank O. Simonin for fruitful discussions and G. Couteau for technical support.

References

[1]Johari, H., and Paduano, R., "Dilution and Mixing in an Unsteady Jet," *Experiments in Fluids*, Vol. 23, 1997, pp. 272–280.

[2]Fiedler, H., "Control of Free Turbulent Shear Flows," *Flow Control—Fundamentals and Practices*, edited by M. Gad-el-Hak, A. Pollard, and J. P. Bonnet, Springer, Berlin, 1998, pp. 335–449.

[3]Marinet, F., and Binder, "Structure des Jets Pulsants," *Journal de Mécanique*, Vol. 18, No. 2, 1979.

[4]Raud, N., Bury, Y., Bazile, R., Borée, J., and Charnay, G., "Experimental Study of the Behavior of Confined Variable Density Jets in a Time Varying Crossflow," *Journal of Fluids Engineering*, Vol. 121, No. 1, 1999, pp. 65–73.

[5]Bury, Y., "Structure de Jets Légers ou Lourds en Écoulement Externe Fortement Pulsé—Expérimentation Modéle du Mélange de Carburants Gazeux dans les Moteurs Alternatifs," Ph.D. Dissertations, Institut National Polytechnique de Toulouse, Toulouse, France, 2000.

[6]Lehmann, B., "Laser-Doppler-Messungen in einem turbulenten Freistrahl," *DFVLR-Forschungsbericht*, Vol. 86-55, 1986.

[7]Curtet, R., and Craya, A., "Sur l'Écoulement d'un Jet Entre Parois," Technical Rept 359, Publications Scientifiques et Techniques du Ministe de l'Air, 1960.

[8]Maczynski, J., "A Round Jet in an Ambient Co-Axial Stream," *Journal of Fluid Mechanics*, Vol. 13, 1961, pp. 597–608.

[9]Bradbury, L., and Riley, J., "The Spread of a Turbulent Plane Issuing into a Parallel Moving Airstream," *Journal of Fluid Mechanics*, Vol. 27, No. 2, 1967, pp. 381–394.

[10]Nickels, T., and Perry, A., "An Experimental and Theorical Study of the Turbulent Coflowing Jet," *Journal of Fluid Mechanics*, Vol. 309, 1996, pp. 157–182.

[11]Wygnanski, I., and Fiedler, H., "Some Measurements in the Self Preserving Jet," *Journal of Fluid Mechanics*, Vol. 38, No. 3, 1969, pp. 577–612.

[12]Hussein, H., Capp, S., and George, W., "Velocity Measurements in a High-Reynolds-Number, Momentum Conserving, Axisymmetric, Turbulent Jet," *Journal of Fluid Mechanics*, Vol. 258, 1994, pp. 31–75.

[13]Antonia, R., and Bilger, R., "An Experimental Investigation of an Axisymmetric Jet in a Co-Flowing Air Stream," *Journal of Fluid Mechanics*, Vol. 61, 1973, pp. 805–822.

[14]Tenekees, H., and Lumley, J., *A First Course in Turbulence*, MIT Press, Cambridge, MA, 1972.

[15]Saudreau, M., "Analyse de la Dynamique des Jets á Densité Variable en Écoulement Cocourant Pulsé," Ph.D. Dissertation, No. 1873, Institut National Polytechnique de Toulouse, Toulouse, France, 2002.

[16]Pope, B., *Turbulent Flows*, Cambridge Univ. Press, Cambridge, England, U.K., 2000.

[17]Bremhorst, K., and Hollis, P. G., "Velocity Field of an Axisymmetric Pulsed, Subsonic Air Jet," *AIAA Journal*, Vol. 28, 1990, pp. 2043–2049.

[18]Borée, J., Atassi, N., and Charnay, G., "Phase Averaged Velocity Field in an Axisymmetric Jet Subject to a Sudden Velocity Decrease," *Experiments in Fluids*, Vol. 21, 1996, pp. 447–456.

[19]Zhang, Q., and Johari, H., "Effects of Acceleration on Turbulent Jets," *Physics of Fluids*, Vol. 8, No. 8, 1996, pp. 2185–2195.

[20]Witze, P., "The Impulsively Started Incompressible Turbulent Jet," Sandia National Labs., Technical Rept., Oct. 1980.

[21]Dimotakis, P. E., "Two-Dimensional Shear-Layer Entrainment," *AIAA Journal*, Vol. 24, 1986, p. 1791.

[22]Kato, S. M., Groenewegen, B. C., and Breidenthal, R. E., "Turbulent Mixing in Nonsteady Jets," *AIAA Journal*, Vol. 25, 1987, pp. 165–168.

[23]Spalart, P., "Strategies for Turbulence Modelling and Simulations," *International Journal of Heat and Fluid Flow*, Vol. 21, 2000, pp. 252–263.

[24]Donghee, H., and Mungal, M., "Direct Measurement of Entrainment in Reacting/Nonreacting Turbulent Jets," *Combustion and Flame*, Vol. 124, 2001, pp. 370–386.

P. Givi
Associate Editor